Evaluation of Collimators in a High-Resolution, Whole-Body SPECT/CT Device with a Dual-Head Cadmium–Zinc–Telluride Detector for ^{123}I-FP-CIT SPECT

Hitoshi Hiraki[1], Toshimune Ito[2], Masahisa Onoguchi[1], Hirotatsu Tsuchikame[3], Masaaki Shishido[3], Takafumi Maeno[3], Takayuki Shibutani[1], and Hiroki Sanada[4]

[1]Department of Quantum Medical Technology, Graduate School of Medical Sciences, Kanazawa University, Kanazawa, Japan; [2]Department of Radiological Technology, Faculty of Medical Technology, Teikyo University, Tokyo, Japan; [3]Department of Radiology, Saiseikai Yokohamashi Tobu Hospital, Yokohama, Japan; and [4]Department of Central Radiology, Teikyo University Mizonokuchi Hospital, Kawasaki, Japan

The study aim was to evaluate the adaptation of collimators to ^{123}I-*N*-fluoropropyl-2b-carbomethoxy-3b-(4-iodophenyl)nortropane (^{123}I-FP-CIT) dopamine transporter SPECT (DAT-SPECT) by a high-resolution whole-body SPECT/CT system with a cadmium–zinc–telluride detector (C-SPECT) in terms of image quality, quantitation, diagnostic performance, and acquisition time. **Methods:** Using a C-SPECT device equipped with a wide-energy, high-resolution collimator and a medium-energy, high-resolution sensitivity (MEHRS) collimator, we evaluated the image quality and quantification of DAT-SPECT for an anthropomorphic striatal phantom. Ordered-subset expectation maximization iterative reconstruction with resolution recovery, scatter, and attenuation correction was used, and the optimal collimator was determined on the basis of the contrast-to-noise ratio (CNR), percentage contrast, and specific binding ratio. The acquisition time that could be reduced using the optimal collimator was determined. The optimal collimator was used to retrospectively evaluate diagnostic accuracy via receiver-operating-characteristic analysis and specific binding ratios for 41 consecutive patients who underwent DAT-SPECT. **Results:** When the collimators were compared in the phantom verification, the CNR and percentage contrast were significantly higher for the MEHRS collimator than for the wide-energy high-resolution collimator ($P < 0.05$). There was no significant difference in the CNR between 30 and 15 min of imaging time using the MEHRS collimator. In the clinical study, the areas under the curve for acquisition times of 30 and 15 min were 0.927 and 0.906, respectively, and the diagnostic accuracies of the DAT-SPECT images did not significantly differ between the 2 times. **Conclusion:** The MEHRS collimator provided the best results for DAT-SPECT with C-SPECT; shorter acquisition times (<15 min) may be possible with injected activity of 167–186 MBq.

Key Words: ^{123}I-FP-CIT; whole-body CZT semiconductor detector; WEHR collimator; MEHRS collimator

J Nucl Med Technol 2023; 51:227–234
DOI: 10.2967/jnmt.122.265328

In Parkinson syndrome, including Parkinson disease and dementia with Lewy bodies, dopamine transporters are present in the terminal portions of nigrostriatal dopaminergic nerves, and the loss of these nerves decreases dopamine transporter expression (*1,2*). To image the presence of these nigrostriatal dopaminergic nerves, ^{123}I-*N*-fluoropropyl-2b-carbomethoxy-3b-(4-iodophenyl)nortropane (^{123}I-FP-CIT) dopamine transporter SPECT (DAT-SPECT), which has a high affinity for dopamine transporters, is performed and is one of the most useful tests for diagnosing Parkinson syndrome, including Parkinson disease and dementia with Lewy bodies (*3–5*). A NaI scintillation detector–equipped Anger-type SPECT (A-SPECT) device, which is a device that uses 2 or 3 detectors (*6*), has been applied to conduct DAT-SPECT studies. To obtain sufficient counts in DAT-SPECT with A-SPECT, an acquisition time of about 30 min is required, even with 3 detectors (*7*). Recently, γ-cameras equipped with cadmium–zinc–telluride (CZT) detectors have been developed and shown to be useful in reducing acquisition time and providing reliable image quality (*8–11*). SPECT systems equipped with CZT detectors were initially developed exclusively for cardiac applications (*12–16*); however, they are beginning to be widely used in clinical practice as a 2-detector whole-body SPECT/CT system (C-SPECT), and C-SPECT systems have demonstrated superior energy resolution and improved high-contrast resolution for each nuclide, as reported in a performance evaluation comparing them with A-SPECT (*17*).

In addition to the standard wide-energy, high-resolution (WEHR) collimator for low- and medium-energy applications, a medium-energy, high-resolution sensitivity (MEHRS) collimator has recently been developed for C-SPECT, and the physical characteristics of C-SPECT and a performance evaluation of the WEHR and MEHRS collimators have been reported (*17*). MEHRS is expected to improve imaging accuracy by reducing the effects of high-energy γ-rays. Consequently, the use of C-SPECT in DAT-SPECT is expected to improve image quality and shorten acquisition times.

Received Dec. 22, 2022; revision accepted Apr. 27, 2023.
For correspondence or reprints, contact Masahisa Onoguchi (onoguchi@staff.kanazawa-u.ac.jp).
Published online Jul. 11, 2023.

However, to the best of our knowledge, no study has comprehensively evaluated the adaptability of collimators in C-SPECT to DAT-SPECT based on the striatal phantoms and clinical studies. This study aimed to evaluate the C-SPECT collimators in DAT-SPECT in terms of image quality, quantity, diagnostic performance, and acquisition time using striatal phantoms and clinical studies.

MATERIALS AND METHODS

SPECT/CT Scanner and Data Acquisition

We used the Discovery NM/CT 870 CZT device equipped with a whole-body CZT detector (GE Healthcare). A C-SPECT device equipped with WEHR and MEHRS collimators was used to acquire all the SPECT data. The design parameters of the WEHR and MEHRS collimators are shown in Table 1 (*17*). Projection data were acquired with a rotation radius of 14 cm using step-and-shoot mode with 360° of rotation in 120 angular views. First, 30 and 15 min of acquisition were performed with each collimator. Second, a 30-min acquisition was performed using each collimator, and data were collected every 5, 10, 15, 20, 25, and 30 min for image reconstruction, which was performed using the Lister tool (GE Healthcare) function for data with an acquisition time of 30 min. The Lister tool function allows image reconstruction with data from any acquisition time within the total acquisition time.

The matrix size was 128 × 128, with 3.32 × 3.32 mm pixels (×1.33 magnification). The photopeak window of ^{123}I was set as a 15% energy window centered on 159 keV. The triple-energy-window method was used for scatter correction (*18,19*), and a lower subwindow of 3% (142.3–147.1 keV) and an upper subwindow of 3% (170.9–175.7 keV) were set for the ^{123}I main peak (*17*). The image-processing system Xeleris 4.0 (GE Healthcare) was used for image reconstruction of the acquired data. For image analysis, we used the general image-processing software ImageJ (National Institutes of Health), Demon Research Image Processor (version 3.01; Fujifilm Toyama Chemical Co.), and DatView (Nihon Medi-Physics, Inc.). The CT imaging parameters used for phantom attenuation correction were as follows: tube voltage, 120 kVp; tube current, 300 mA; detector configuration, 16 × 0.625 mm; rotation time, 0.8 s; slice thickness, 5 mm; and pitch, 0.938. For attenuation correction of the clinical data, the tube current was set to 30 mA.

Phantom Study

Phantom. An anthropomorphic striatal phantom, DaT1308 (NMP Business Support Co., Ltd.), was used as the phantom to acquire projection data (Supplemental Fig. 1; supplemental materials are available at http://jnm.snmjournals.org). The first projection data showed that the left and right striatum and background of the phantom were filled with ^{123}I solution with a radioactivity ratio of about 8:1 (striatum, 40.0×10^3 Bq/mL; background, 5.0×10^3 Bq/mL; striatum-to-background ratio, 8.0), assuming a very normal one (*20,21*). The second projection data showed that the left and right striatum and background of the phantom were filled with an approximately 4:1 ^{123}I solution, assuming a very low radioactivity ratio (striatum, 20.0×10^3 Bq/mL; background, 5.0×10^3 Bq/mL; striatum-to-background ratio, 4.0) (*20,21*).

Image Reconstruction. The phantom image was reconstructed using ordered-subset expectation maximization iterative reconstruction with resolution recovery, scatter correction, and attenuation correction (OSEMRRSCAC; subsets, 6; iterations, 15). Attenuation and scatter correction were by the triple-energy-window method (*18*), and resolution recovery was according to the report on optimization of reconstruction conditions in A-SPECT by Matsutomo et al. (*19*). A lower subwindow of 3% (142.3–147.1 keV) and an upper subwindow of 3% (170.9–175.7 keV) were set for the ^{123}I main peak. Post-Butterworth filtering (power, 16; cutoff, 0.5 cycle/cm) was used as the smoothing process (*22*). The CT attenuation correction method was used for attenuation correction.

Phantom Collimator Evaluation. To investigate the basic features of the different collimators, we calculated the contrast-to-noise ratio (CNR) and percentage contrast for different radioactivity ratios (8:1 vs. 4:1) of the striatum to the collimator and different acquisition times (30 and 15 min). First, a striatal region of interest (ROI) was manually contoured and placed on the CT image using the method reported by Matsutomo et al. (*19*). The ROIs were then copied onto the SPECT images (*19*). The striatum was measured using 12 ROIs in the left and right caudate nuclei and putamen for each of the 3 cross-sectional images (Supplemental Fig. 1). A rectangular 1,940 mm^2 background ROI was placed at the back of the phantom; the CNR and percentage contrast were then calculated using Equations 1 and 2:

$$\mathrm{CNR} = (\overline{C}_{\mathrm{striatum}} - \overline{C}_{\mathrm{bg}})/\overline{\mathrm{SD}}_{\mathrm{bg}} \quad \text{Eq. 1}$$

$$\%\ \mathrm{contrast} = (\overline{C}_{\mathrm{striatum}}/\overline{C}_{\mathrm{bg}})/(\text{striatal count ratio: theoretical value}) \times 100, \quad \text{Eq. 2}$$

where $\overline{C}_{\mathrm{striatum}}$ is the mean count in the striatum ROI, $\overline{C}_{\mathrm{bg}}$ is the mean count in the background ROI, and $\overline{\mathrm{SD}}_{\mathrm{bg}}$ is the mean of the SD of the background ROI. The striatal count ratio is 8 or 4, which is the striatal radioactivity count ratio, and the theoretic value is 1, which is the background radioactivity count ratio.

The quantitative performance of the collimator was evaluated by measuring the specific binding ratio (SBR) of the phantom images according to the method reported by the team of Tossici-Bolt (*22,23*). The SBR is defined as the ratio of the specific binding concentration of the tracer in the striatum to the nonspecific binding concentration in all brain regions. This method uses a semiautomatic analysis and comprises 3 functions: manual placement of the whole striatal volume of interest (VOI), automated creation of a reference VOI, and calculation of SBR. First, the whole striatal VOI was set for the summed images oriented to the orbitomeatal plane.

TABLE 1
Collimator Designs

Collimator	Type of hole	Hole length (mm)	Hole diameter (mm)	Septal thickness (mm)	Number of holes	Penetration (%)
WEHR	Square	45	2.26	0.2	33,280	0.55 (^{99m}Tc)
MEHRS	Hexagonal	40.25	2.8	0.9	Undisclosed	1.8 (^{111}In)

Second, the reference VOI for the estimation of the nonspecific count was set for the whole brain with the exclusion of the striatum. Finally, the SBR was calculated using Equation 3:

$$SBR = (1/V_s)\{Ct_{VOI}/C_r - V_{VOI}\}, \quad \text{Eq. 3}$$

where V_s is the standard volume of the striatum (11.2 mL), Ct_{VOI} is the total count in the striatal VOI, C_r is the count concentration in a reference VOI, and V_{VOI} is the volume of the striatal VOI. Because the striatal-to-background radioactivity ratios were 8:1 and 4:1, the SBRs calculated using the true radioactivity were 7 and 3 for 8:1 and 4:1, respectively.

Short-Acquisition-Time Collection Evaluation for Phantom. The Lister tool function for data with an acquisition time of 30 min was used to perform image reconstructions for the acquisition times of 5, 10, 15, 20, 25, and 30 min, and the CNR, percentage contrast, and SBR were then calculated and evaluated.

Clinical Study

Clinical Subjects. We retrospectively examined the imaging data of 41 consecutive patients who had previously undergone DAT-SPECT with the MEHRS collimator, including 10 patients in the normal-accumulation group and 31 patients in the decreased-accumulation group for DAT-SPECT. This clinical evaluation was performed by 2 experienced radiologists according to established consensus criteria for the diagnosis of each disease, factoring in morphologic information from MRI or CT images performed at approximately the same time as DAT-SPECT. The patients comprised 23 men and 18 women, with ages ranging from 40 to 86 y (mean, 71.9 ± 11.4 y). An equivalent to the institutional review board approved this retrospective study, and the requirement to obtain informed consent was waived.

Clinical SPECT Protocol. ^{123}I-FP-CIT (167 MBq, 167–186 MBq) was intravenously injected into each patient. Data acquisition started about 4 h after administering ^{123}I-FP-CIT, with an imaging duration of 30 min (*7,24*). Immediately after DAT-SPECT, a low-dose CT scan was performed using the same parameters as in the phantom study. The CT imaging parameters used for attenuation correction of the clinical data were as follows: tube voltage, 120 kVp; tube current, 30 mA; detector configuration, 16 × 0.625 mm; rotation time, 0.8 s; slice thickness, 5 mm; and pitch, 0.938. DAT-SPECT images were reconstructed using the OSEMRRSCAC algorithm. The imaging time parameters used for reconstruction were determined from the phantom study.

Clinical Diagnostic Accuracy. The images were reconstructed with an acquisition time of 30 min and another acquisition time determined via phantom verification. The SBRs were calculated from the reconstructed images and compared. The diagnostic accuracies of these 2 images were then evaluated according to the receiver-operating-characteristic (ROC) analysis. Using a continuous confidence rating method, the ROC analysis assessed the degree of accumulation in the striatum on a free scale from the decreased-accumulation group to the normal-accumulation group. The quality of DAT-SPECT images was visually assessed by 2 board-certified nuclear medicine physicians and 5 board-certified nuclear medicine technologists. The ROC analysis was completed by averaging the results for these observers.

Statistical Analysis

The CNR, percentage contrast, and SBR results from the phantom study were compared using the Shapiro–Wilk test, paired *t* test, Wilcoxon test, 1-way ANOVA, and Friedman test. Multireader, multicase ANOVA according to the jackknife method and tests with 95% CIs were used to compare the ROC curves for the clinical study (*25*). *P* values of less than 0.05 were considered to indicate statistical significance.

RESULTS

Phantom Study

Collimator Evaluation Results. The phantom images are shown in Figure 1. The CNR and percentage contrast are shown in Figures 2 and 3. The CNR was significantly higher for the MEHRS collimator than for the WEHR collimator ($P < 0.05$). The percentage contrast did not significantly differ between the collimators for the 30-min acquisition time and the radioactivity ratio of 8:1. However, in other cases, the MEHRS collimator had significantly higher values ($P < 0.05$). Considering a theoretic value of 7 for the SBR, the SBR values of the MEHRS and WEHR collimators were 9.27 and 8.85, respectively, for the 30-min collection and 9.15 and 8.89, respectively, for the 15-min collection. Similarly, considering the theoretic SBR value of 3, the SBR values of the MEHRS and WEHR collimators were 3.72

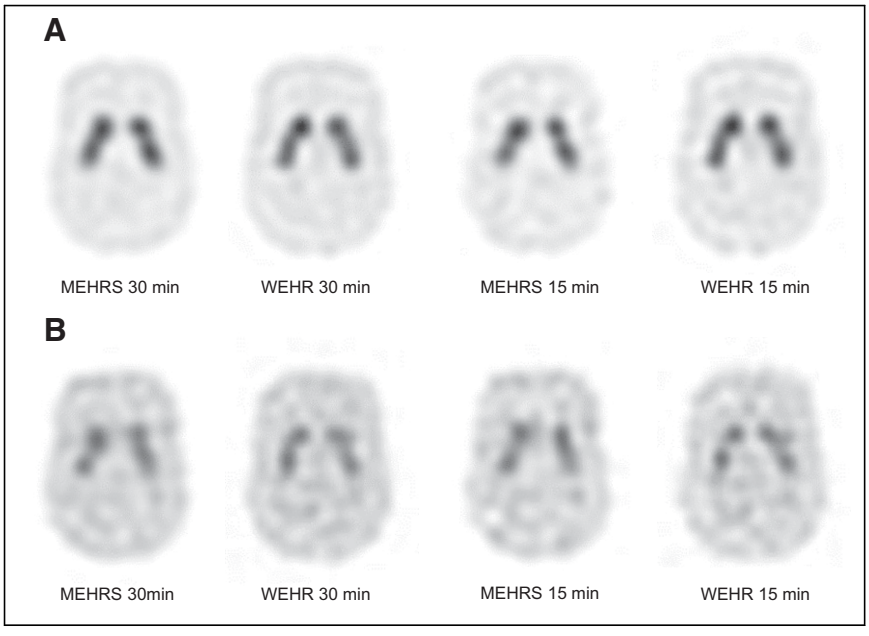

FIGURE 1. DAT-SPECT images of anthropomorphic striatal phantom with different collimators, acquisition times, and striatum-to-background radiation ratios. Phantom's striatum and background were bilaterally filled with ^{123}I solution at radioactivity ratios (Bq/mL) of ~8:1 (A) and ~4:1 (B).

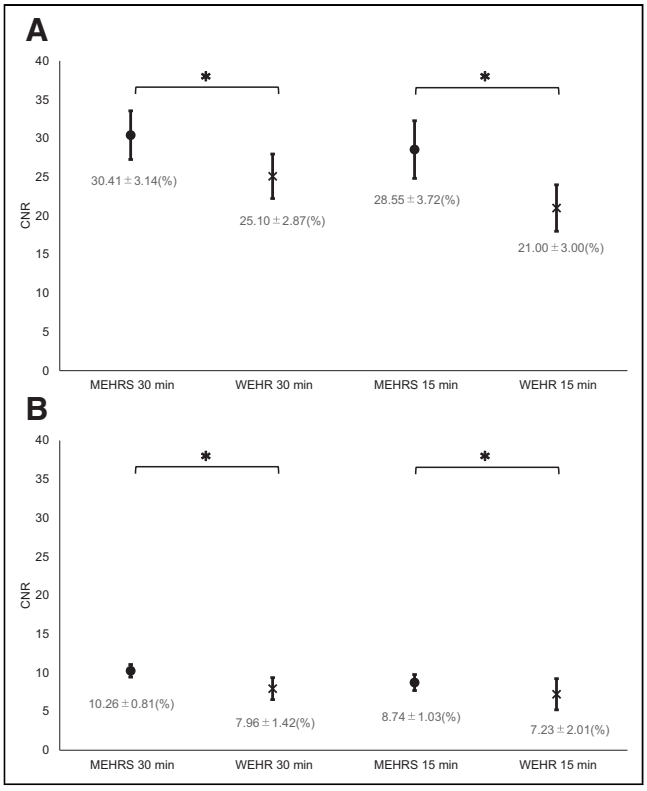

FIGURE 2. CNR of DAT-SPECT images of anthropomorphic striatal phantom with different collimators, acquisition times, and striatum-to-background radiation ratios. (A) Images with radioactivity ratio (Bq/mL) of ~8:1. (B) Images with radioactivity ratio (Bq/mL) of ~4:1. *$P < 0.05$.

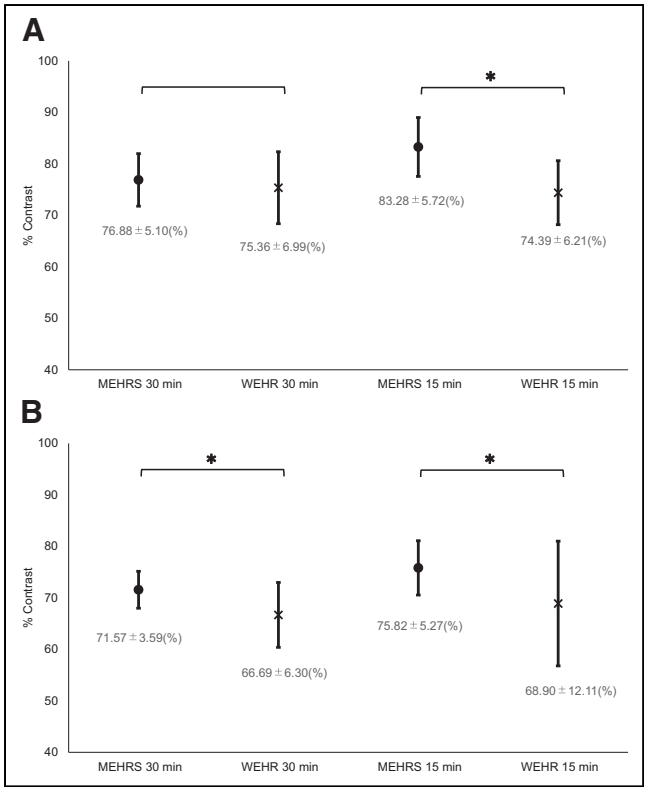

FIGURE 3. Percentage contrast of DAT-SPECT images of anthropomorphic striatal phantom with different collimators, acquisition times, and striatum-to-background radiation ratios. (A) Images with radioactivity ratio (Bq/mL) of ~8:1. (B) Images with radioactivity ratio (Bq/mL) of ~4:1. *$P < 0.05$.

and 3.34, respectively, for the 30-min collection and 4.06 and 3.47, respectively, for the 15-min collection. Both collimators had higher SBR values than the theoretic values, but the MEHRS collimator's value was the highest.

Evaluation Results of Short-Acquisition-Time Collection. A collimator chosen according to the results of the phantom evaluation was used for validating the short acquisition time in DAT-SPECT. We compared the images from the standard 30-min acquisition time with those from the short acquisition time. The phantom images are shown in Figure 4, and the CNRs and percentage contrast are in Figures 5 and 6. Regarding CNRs, at a radioactivity ratio of 8:1, only the 5-min acquisition time afforded significantly different CNRs from that for the 30-min acquisition time ($P < 0.05$). At a radioactivity ratio of 4:1, there was a significant difference in the CNRs between the 5- and 10-min acquisitions, compared with that for the 30-min acquisition ($P < 0.05$). Regarding percentage contrast, at a radioactivity ratio of 8:1, only the 10- and 15-min acquisitions afforded percentage contrasts significantly different from that for the 30-min acquisition ($P < 0.05$). At a radioactivity ratio of 4:1, there was no significant difference in percentage contrasts among all the acquisition times. The SBRs are shown in Table 2. For the radioactivity ratio of 8:1, the SBR values ranged from 9.14 to 9.92 depending on the acquisition times, whereas the theoretic SBR was 7. The SBR with an acquisition time of 5 min was highest, at 9.92. For the radioactivity ratio of 4:1, the SBR values ranged from 3.72 to 4.37 with different acquisition times, whereas the theoretic value was 3. The SBR with an acquisition time of 10 min was highest, at 4.37.

Clinical Study

Figure 7 shows a comparison of SBRs obtained at acquisition times of 30 and 15 min in DAT-SPECT using the MEHRS collimator. The SBR values remained stable across all studied subjects, with correlations of at least 0.98 at 30 and 15 min of acquisition time, with no significant difference.

The results of the ROC analysis to differentiate between the normal-accumulation and decreased-accumulation groups are shown in Figure 7. The areas under the ROC curve for the 30- and 15-min acquisition times were 0.927 and 0.906, respectively, but the differences were not significant.

DISCUSSION

In this study, we evaluated collimator adaptation for C-SPECT in DAT-SPECT. For collimator verification in the phantom study, we first used the WEHR and MEHRS collimators with radioactivity ratios of 8:1 and 4:1 and acquisition times of 30 and 15 min for the striatum and then evaluated the image quality and quantification. Based on the characteristics

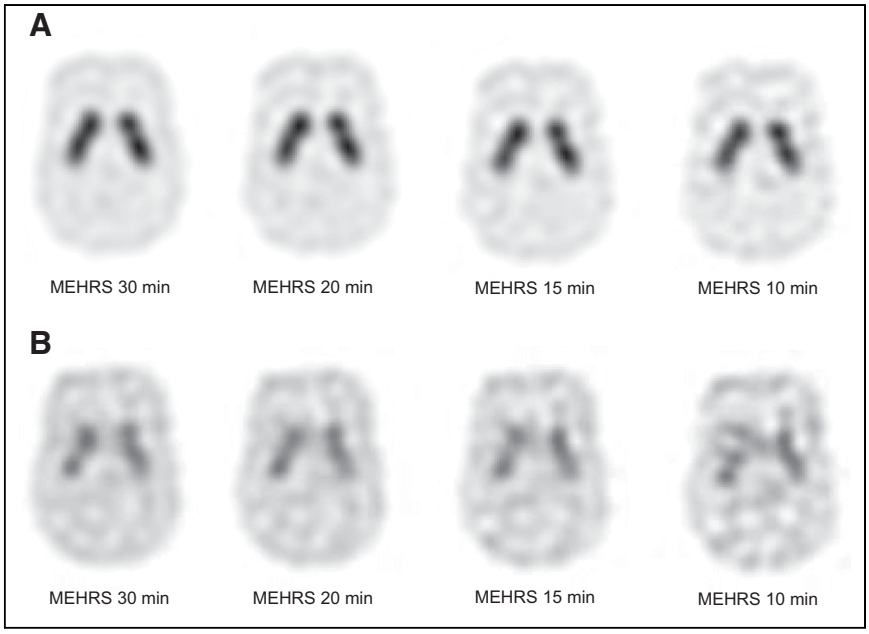

FIGURE 4. DAT-SPECT images using MEHRS collimator with different acquisition times (10, 15, 20, and 30 min). (A) Images with radioactivity ratio (Bq/mL) of ~8:1. (B) Images with radioactivity ratio (Bq/mL) of ~4:1.

of the WEHR and MEHRS collimators in C-SPECT by Ito et al. (*17*), because of the incomplete charge acquisition of the electron–hole pair and intercrystal scattering in C-SPECT, the scattering component increases as a result of the effects of hole tailing in the Compton region. This result suggests that the scattered component increases because of the 529-keV septum penetration of ^{123}I and the hole tailing in the Compton region and scattering between crystals. The MEHRS collimator has a thick septum to reduce the scattered radiation component. Furthermore, the MEHRS collimator could acquire primary photons with higher accuracy using the appropriate triple-energy-window method, which is thought to improve image uniformity, and the MEHRS collimator provided significantly higher CNR values.

The percentage contrast showed the same trend as the CNR results.

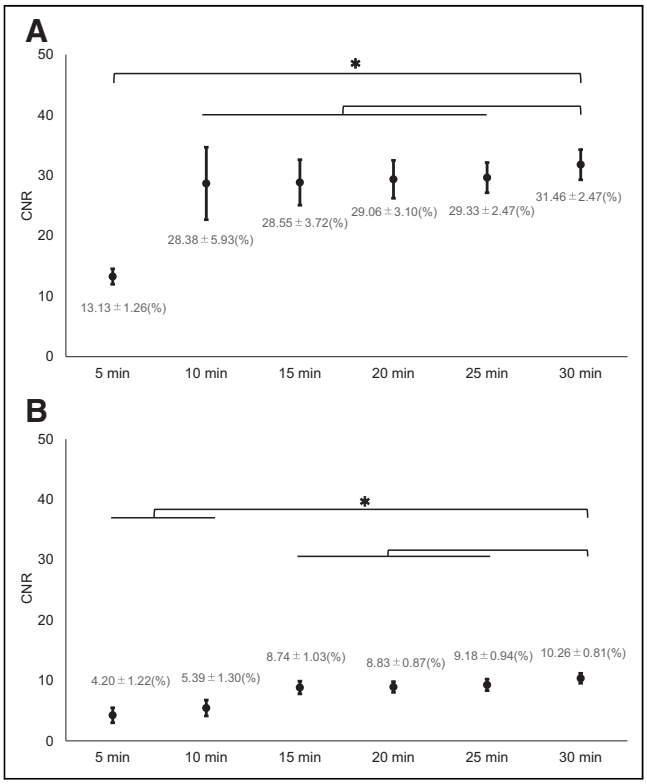

FIGURE 5. CNR of DAT-SPECT images using MEHRS collimator with different acquisition times (10, 15, 20, and 30 min). (A) Images with radioactivity ratio (Bq/mL) of ~8:1. (B) Images with radioactivity ratio (Bq/mL) of ~4:1. *$P < 0.05$.

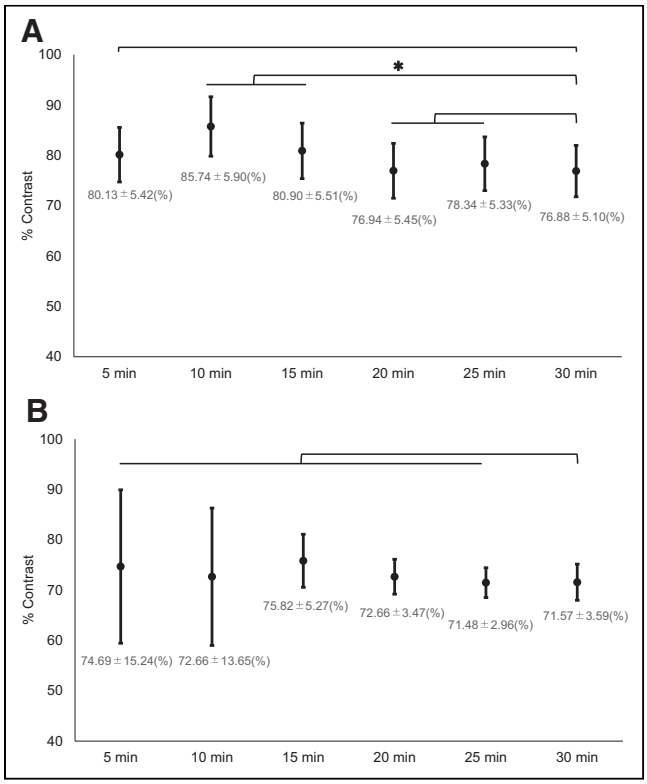

FIGURE 6. Percentage contrast of DAT-SPECT images using MEHRS collimator with different acquisition times (10, 15, 20, and 30 min). (A) Images with radioactivity ratio (Bq/mL) of ~8:1. (B) Images with radioactivity ratio (Bq/mL) of ~4:1. *$P < 0.05$.

TABLE 2
SBR of DAT-SPECT Images Using MEHRS Collimator with Different Acquisition Times

Radioactivity ratio	SBR					
	5 min	10 min	15 min	20 min	25 min	30 min
8:1	9.92	9.30	9.15	9.14	9.41	9.27
4:1	3.73	4.37	4.06	3.83	3.78	3.72

This result may be attributed to the removal of the scattered component and acquisition of primary photons (*17*). At an acquisition time of 30 min and a striatal radioactivity ratio of 8:1, no significant difference was observed in percentage contrast because sufficient counts were obtained at both collimators because of the adequate acquisition time and high striatal accumulation radioactivity ratio.

The SBR has been reported by Meyer et al. to depend on the imaging parameters, such as the device used for imaging, type of collimator, and image reconstruction parameters (*26*). In this study, the SBRs were higher in C-SPECT than the theoretic value for both the WEHR and MEHRS collimators.

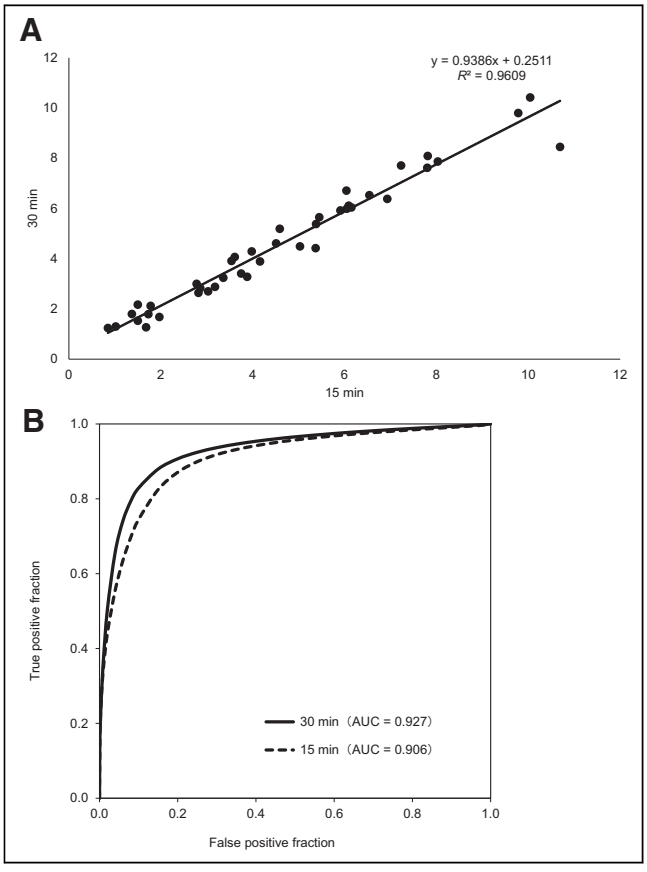

FIGURE 7. (A) Correlation between SBR values ≥ 0.98 at 30- and 15-min acquisition times. (B) Comparison of average ROC curves for differentiation between normal-accumulation group and decreased-accumulation group. For both A and B, difference is not statistically significant. AUC = area under the ROC curve.

The SBRs were higher in the MEHRS collimator than those in the WEHR collimator. Ito et al. showed that the energy resolution in C-SPECT was 1.67 times higher when using the MEHRS collimator than with the WEHR collimator (*17*). The background ROI counts were lower for both WEHR and MEHRS collimators because of the effects of septum penetration and hole tailing of scattered rays, which are the same reasons as those for CNR and percentage contrast. The striatum counts were higher for the MEHRS collimator because of the acquisition of primary photons. The SBR was higher than the theoretic value for both collimators, with the MEHRS collimator showing a higher value. In addition, Matsuda et al. reported that the SBR was higher under scatter correction conditions than without scatter correction (*21*), and the results were comparable for C-SPECT. The CNR, percentage contrast, and SBR values show that the MEHRS collimator is optimal for use in DAT-SPECT in C-SPECT.

Then, to validate a short acquisition time, based on the results obtained from the collimator validation, images were acquired using the MEHRS collimator with a 30-min acquisition time. Further, the Lister tool function was used to reconstruct images for 5, 10, 15, 20, 25, and (the reference) 30 min (Fig. 4) to evaluate image quality and quantification. There were no significant differences in CNRs for the 8:1 radioactivity ratio of the striatum over 10 min or for the 4:1 radioactivity ratio of the striatum over 15 min (Fig. 5).

According to a study by Bailly et al. validating A-SPECT with an injected activity of 185 MBq of Swiftscan (GE Healthcare), a 25% reduction in acquisition time from 30 min was possible (*27*). In a study by Bani Sadr et al. using a WEHR collimator for C-SPECT at an injected activity of 185 MBq, the image quality and SBR values were stable from 30 to 15 min of acquisition time, indicating that a 2-fold reduction in acquisition time was possible (*11*). The validation of the collimator in C-SPECT showed that the acquisition time could be reduced from that of A-SPECT using Swiftscan, which was consistent with the results using the WEHR collimator in C-SPECT, and that the acquisition time of 15 min was also possible for the striatum radioactivity ratio (8:1 and 4:1).

The 8:1 radioactivity ratio of the striatum afforded a significantly higher percentage contrast only at 10 and 15 min ($P < 0.05$), and there was no significant difference in the values when the acquisition times were 5 and 20 min or longer. There was no significant difference in the percentage contrast values for the radioactivity ratio of the striatum of 4:1 at any acquisition times (Fig. 6). As the activity and detection efficiency increase (i.e., the more counts [photons] used in image formation), the contrast increases because the proportion of noise components in the image decreases (*28*). For the 8:1 radioactivity ratio of the striatum, the extremely short acquisition time of 5 min resulted in low background counts and consequently did not provide significantly different results from the those obtained at an acquisition time of 30 min, and the results for the acquisition times of 20 and 25 min were not significantly different because of the

sufficient counts obtained. However, at acquisition times of 10 and 15 min, the percentage contrast values were significantly higher because the MEHRS collimator has a thicker septum to remove scattered radiation components; furthermore, using the appropriate triple-energy-window method, primary photons can be acquired with high accuracy, improving uniformity and suppressing background counts relative to the increase in striatal counts. The 4:1 radioactivity ratio of the striatum resulted in a larger proportion of noise components in the image because of the small number of counts (photons) used for image formation and the very small number of counts of the striatum in the acquisitions up to 30 min, indicating that overall, no significant differences were detected. We observed some statistically significant differences in percentage contrast for varying acquisition times at the 8:1 striatum radioactivity ratio. However, it was difficult to provide a threshold acquisition time.

Next, we discuss the SBR for acquisition time variation. Bani Sadr et al. showed that SBR does not vary significantly with reducing the acquisition time (*11*). However, in the present verification, the SBRs were the highest for the 5- and 10-min acquisition times at the 8:1 and 4:1 radioactivity ratio of the striatum, respectively. The SBR changed the most between the 5- and 10-min acquisition times. The method reported by Tossici-Bolt et al. uses a 3-dimensional ROI that is sufficiently larger than the striatal volume to eliminate partial-volume effects of the striatum and interanalyst errors (*23*). Thus, the changes observed at the 8:1 striatal radioactivity ratio could be related to the effect of acquiring more primary photons because of the higher radioactivity of the striatum for extremely short acquisition times (*17*), whereas the changes observed at a 4:1 striatal radioactivity ratio could be related to the stronger effect of count variations due to fewer counts in the striatum and in the background brain parenchyma. On the basis of the CNR results, we determined that the acquisition time for an injected activity of 167–186 MBq could be reduced to 15 min.

In the clinical study, based on the results obtained from the phantom validation, the SBR was calculated using C-SPECT with a MEHRS collimator and the 30-min reference acquisition time. Similarly, the SBR was calculated and evaluated using images with a 15-min acquisition time based on the results obtained from the phantom validation. The obtained result is consistent with the results presented by Bani Sadr et al., who reported no significant differences in SBRs with reduced acquisition times (*11*). In addition, Ito et al. showed that when ^{123}I is used for C-SPECT, by setting an appropriate scattering window and performing scattering correction, it is possible to acquire primary photons with high accuracy and an excellent scatter removal effect, which enables highly uniform imaging while maintaining high-contrast resolution (*17*). As a result, uniform imaging was possible even at a 15-min acquisition time, which is considered to be an SBR that is not significantly different from that obtained at a 30-min acquisition time.

Second, there were no significant differences in visual evaluation. Bani Sadr et al. showed that DAT-SPECT using a WEHR collimator for C-SPECT provides reliable image quality and a reliable diagnosis for an acquisition time of 15 min (*11*) and that images with an acquisition time of 15 min, which was not significantly different from the standard acquisition time of 30 min using a MEHRS collimator for C-SPECT, are considered to be available for diagnosis.

These results are consistent with the report by Ito et al., who suggested that using a MEHRS collimator for C-SPECT is suitable for ^{123}I imaging, and it is assumed that the use of a MEHRS collimator for C-SPECT improves the image quality of DAT-SPECT compared with a WEHR collimator (*17*). In addition, a study by Bani Sadr et al. showed that the acquisition time of 15 min is possible using a WEHR collimator for C-SPECT (*11*), which is consistent with the results obtained using a MEHRS collimator for C-SPECT, which showed that an acquisition time of 15 min was possible, and it was assumed that the acquisition time can be shortened.

The present study had some limitations. First, we cited the report of Matsutomo et al., who used A-SPECT for reconstruction parameters (*19*). Furthermore, Onishi et al. reported that the optimal reconstruction parameters differ depending on the available iterative reconstruction techniques (*29*). Therefore, the best reconstruction parameters in C-SPECT may differ and it is necessary to validate the reconstruction parameters in C-SPECT. If the best reconstruction parameters are found, it may be possible to improve the image quality of DAT-SPECT in C-SPECT and further reduce acquisition times.

Second, the number of subjects was limited in the clinical study. Matsuda et al. suggested that the ratio of a specific striatum to nonspecific ^{123}I-FP-CIT binding decreases considerably with age (*21*). Lavalaye et al. have shown that the binding rate of ^{123}I-FP-CIT is considerably higher in women than in men (*30*). In this validation, the short acquisition time was limited to 15 min based on the results of the phantom validation. However, it is believed that further potential benefits of short acquisition times can be proven by separately evaluating the diagnostic effectiveness from the images of patients with and without a disease. This verification was evaluated on a limited number of 41 patients, which means that it should be evaluated on more than 41 patients.

CONCLUSION

Here, we have demonstrated the adaptation of C-SPECT in DAT-SPECT by first performing a phantom study to determine the optimal collimator for use, which was then applied in a clinical study. Our results indicated that the use of C-SPECT with a MEHRS collimator in DAT-SPECT improved the performance and image quality of DAT-SPECT relative to that of a WEHRS collimator. The results also indicated that the MEHRS collimator could reduce the 30-min acquisition time for DAT-SPECT to 15 min because

there was no statistically significant difference between the 30- and 15-min acquisition times.

DISCLOSURE

No potential conflict of interest relevant to this article was reported.

KEY POINTS

QUESTION: Compared with previous reports on the WEHR collimator, can ^{123}I-FP-CIT SPECT using a CZT detector with a MEHRS collimator improve image quality and reduce acquisition time?

PERTINENT FINDINGS: Phantom validation suggested that the MEHRS collimator improved image quality and potentially reduced acquisition times. Clinical validation in 41 patients suggested that the MEHRS collimator may reduce acquisition time as much as the WEHRS collimator.

IMPLICATIONS FOR PATIENT CARE: The MEHRS collimator is recommended for ^{123}I-FP-CIT SPECT with a CZT detector.

REFERENCES

1. Niznik HB, Fogel EF, Fassos FF, Seeman P. The dopamine transporter is absent in parkinsonian putamen and reduced in the caudate nucleus. *J Neurochem.* 1991;56:192–198.
2. Piggott MA, Perry EK, Marshall EF, et al. Nigrostriatal dopaminergic activities in dementia with Lewy bodies in relation to neuroleptic sensitivity:comparisons with Parkinson's disease. *Biol Psychiatry.* 1998;44:765–774.
3. O'Brien JT, Colloby S, Fenwick J, et al. Dopamine transporter loss visualized with FP-CIT SPECT in the differential diagnosis of dementia with Lewy bodies. *Arch Neurol.* 2004;61:919–925.
4. Booij J, Tissingh G, Boer GJ, et al. ^{123}I FP-CIT SPECT shows a pronounced decline of striatal dopamine transporter labelling in early and advanced Parkinson's disease. *J Neurol Neurosurg Psychiatry.* 1997;62:133–140.
5. Bártová P, Kraft O, Bernátek J, et al. Transcranial sonography and ^{123}I-FP-CIT single photon emission computed tomography in movement disorders. *Ultrasound Med Biol.* 2014;40:2365–2371.
6. Varrone A, Sansone V, Pellecchia MT, et al. Comparison between a dual-head and a brain-dedicated SPECT system in the measurement of the loss of dopamine transporters with [^{123}I]FP-CIT. *Eur J Nucl Med Mol Imaging.* 2008;35:1343–1349.
7. Darcourt J, Booij J, Tatsch K, et al. EANM procedure guidelines for brain neurotransmission SPECT using ^{123}I-labelled dopamine transporter ligands, version 2. *Eur J Nucl Med Mol Imaging.* 2010; 37:443–442.
8. Eisen Y, Shor A, Mardor I. CdTe and CdZnTe x-ray and gamma-ray detectors for imaging systems. *IEEE Trans Nucl Sci.* 2004;51:1191–1198.
9. Spartiotis K, Leppanen A, Pantsar T, et al. A photon counting CdTe gamma- and x-ray camera. *Nucl Inst Institut Methods Phys Res.* 2005;550:267–277.
10. Ogawa K, Ohmura N, Iida H, Nakamura K, Nakahara T, Kubo A. Development of an ultra-high resolution SPECT system with a CdTe semiconductor detector. *Ann Nucl Med.* 2009;23:763–770.
11. Bani Sadr A, Testart N, Tylski P, Scheiber C. Reduced scan time in ^{123}I-FP-CIT SPECT imaging using a large-field cadmium-zinc-telluride camera. *Clin Nucl Med.* 2019;44:568–569.
12. Gambhir SS, Berman DS, Ziffer J, et al. A novel high-sensitivity rapid-acquisition single-photon cardiac imaging camera. *J Nucl Med.* 2009;50:635–643.
13. Garcia EV, Faber TL, Esteves FP. Cardiac dedicated ultrafast SPECT cameras: new designs and clinical implications. *J Nucl Med.* 2011;52:210–217.
14. Verger A, Imbert L, Yagdigul Y, et al. Factors affecting the myocardial activity acquired during exercise SPECT with a high-sensitivity cardiac CZT camera as compared with conventional Anger camera. *Eur J Nucl Med Mol Imaging.* 2014; 41:522–528.
15. Ben-Haim S, Kennedy J, Keidar Z. Novel cadmium-zinc telluride devices for myocardial perfusion imaging: technological aspects and clinical applications. *Semin Nucl Med.* 2016;46:273–285.
16. Niimi T, Nanasato M, Sugimoto M, Maeda H. Evaluation of cadmium-zinc-telluride detector-based single-photon emission computed tomography for nuclear cardiology: a comparison with conventional anger single-photon emission computed tomography. *Nucl Med Mol Imaging.* 2017;51:331–337.
17. Ito T, Matsusaka Y, Onoguchi M, et al. Experimental evaluation of the GE NM/CT 870 CZT clinical SPECT system equipped with WEHR and MEHRS collimator. *J Appl Clin Med Phys.* 2021;22:165–177.
18. Ichihara T, Ogawa K, Motomura N, Kubo A, Hashimoto S. Compton scatter compensation using the triple-energy window method for single and dual-isotope SPECT. *J Nucl Med.* 1993;34:2216–2221.
19. Matsutomo N, Nagaki A, Yamao F, Sasaki M. Optimization of iterative reconstruction parameters with 3-dimensional resolution recovery, scatter and attenuation correction in ^{123}I-FP-CIT SPECT. *Ann Nucl Med.* 2015;29:636–642.
20. Tossici-Bolt L, Dickson JC, Sera T, et al. Calibration of gamma camera systems for a multicentre European ^{123}I-FP-CIT SPECT normal database. *Eur J Nucl Med Mol Imaging.* 2011;38:1529–1540.
21. Matsuda H, Murata M, Mukai Y, et al. Japanese multicenter database of healthy controls for [^{123}I]FP-CIT SPECT. *Eur J Nucl Med Mol Imaging.* 2018;45:1405–1416.
22. Dickson JC, Tossici-Bolt L, Sera T, et al. The impact of reconstruction method on the quantification of DaTSCAN images. *Eur J Nucl Med Mol Imaging.* 2010;37:23–35.
23. Tossici-Bolt L, Hoffmann SM, Kemp PM, Mehta RL, Fleming JS. Quantification of [^{123}I] FP-CIT SPECT brain images: an accurate technique for measurement of the specific binding ratio. *Eur J Nucl Med Mol Imaging.* 2006;33:1491–1499.
24. Djang DS, Janssen MJ, Bohnen N, et al. SNM practice guideline for dopamine transporter imaging with ^{123}I-ioflupane SPECT 1.0. *J Nucl Med.* 2012;53:154–163.
25. Shiraishi J, Fukuoka D, Iha R, Inada H, Tanaka R, Hara T. Verification of modified receiver-operating characteristic software using simulated rating data. *Radiol Phys Technol.* 2018;11:406–414.
26. Meyer PT, Sattler B, Lincke T, Seese A, Sabri O. Investigating dopaminergic neurotransmission with ^{123}I-FP-CIT SPECT: comparability of modern SPECT systems. *J Nucl Med.* 2003;44:839–845.
27. Bailly M, Le Rouzic G, Metrard G, Ribeiro MJ. Faster acquisition for dopamine transporter imaging using Swiftscan step and shoot continuous SPECT without impairing visual and semiquantitative analysis. *Front Med (Lausanne).* 2020;7:235.
28. Kazunori Y. Basic knowledge about diagnostic image quality for beginners. *Dent Radrad.* 2016;56:1–7.
29. Onishi H, Motomura N, Fujino K, Natsume T, Haramoto Y. Quantitative performance of advanced resolution recovery strategies on SPECT images: evaluation with use of digital phantom models. *Radiol Phys Technol.* 2013;6:42–53.
30. Lavalaye J, Booij J, Reneman L, Habraken JB, van Royen EA. Effect of age and gender on dopamine transporter imaging with [^{123}I] FP-CIT SPET in healthy volunteers. *Eur J Nucl Med.* 2000;27:867–869.